Journal of Nuclear Materials 392 (2009) 85–89

Contents lists available at ScienceDirect

Journal of Nuclear Materials

journal homepage: www.elsevier.com/locate/jnucmat

An advanced model for grain face diffusion transport in irradiated UO_2 fuel. Part 2: Model implementation and validation

V.I. Tarasov, M.S. Veshchunov *

Nuclear Safety Institute (IBRAE), Russian Academy of Sciences, 52, B. Tulskaya, Moscow 115191, Russian Federation

A B S T R A C T

The advanced model for intergranular diffusion transport in irradiated UO_2 fuel described in Part 1 is numerically realized. The important model parameters are specified and improvement of the model for the irradiation induced re-solution of gas atoms from the intergranular bubbles is carried out. Implementation of the model in the MFPR code and numerical treatment of various available data on gas release from irradiated fuel and grain face microstructure show a satisfactory agreement of the code predictions with experimental observations. In particular, the main model prediction concerning the onset of gas release from fuel at very low grain face bubble coverage, below the saturation value manifested by formation of bubble network on grain faces, was confirmed by calculations.

1. Introduction

The advanced model for the grain face transport of gas atoms was formulated in Part 1 of the paper that self-consistently takes into consideration the effects of atom diffusion on the grain surface along with trapping by and irradiation-induced re-solution from intergranular bubbles. It is shown that circulation of gas atoms collected by growing intergranular bubbles from the grain face and then returned back (by the re-solution process) into the grain matrix makes intergranular bubbles much less effective sinks for gas atoms and thus increases a fraction of the diffusion flux from the grain directly transported to the grain edges. In particular, this mechanism allows explanation of the observed in the experiment [1,2] a noticeable gas release from fuel when the grain face coverage is far below the critical value, associated in the standard approach with the onset of bubble network on grain faces [3–6].

More detailed description and numerical realisation of the model is described in this paper that relates to specification of the model parameters, introduced in Part 1, including revision of the intergranular bubble nomenclature, their shape and sizes, and modification of the model for the irradiation induced re-solution of gas atoms from the intergranular bubbles.

Furthermore, the model is implemented into the MFPR code [7,8] and fitted to experimental data [1,2]. Results of the model validation against various tests are also presented in this part of the article.

2. Specification of the model parameters

2.1. Extra-granular porosity geometry

From a geometrical point of view, the UO_2 grains can be considered as truncated octahedrons, or tetrakaidecahedrons (TDK) [3]. The TDK has 14 faces, six of which are square and eight hexagonal, 36 edges and 24 corners. When packed together an array of tetrakaidecahedrons (TDKs) can fill all available space in a solid and thus represents an appropriate basic building block. The meeting point of each grain face is shared by two grains, each grain edge by three grains and each grain corner by four grains. Hence, on average each grain has $N_{fpgr} = 7$ faces, $N_{epgr} = 12$ edges and $N_{cpgr} = 6$ corners. Tucker has further rationalized the TDK structure by assuming that the grain is composed of fourteen circular faces with radius $R_{face} = d_{gr}/\sqrt{14}$, where d_{gr} is the grain diameter [9].

The volume V of the TDK is calculated as:

$$V = 8\sqrt{2}L_{edge}^3, \tag{1}$$

where L_{edge} is the grain edge length.

For further simplification, the fuel grains are assumed to be of spherical form. So, equating the sphere volume with the value given by Eq. (1) one derives that:

$$L_{edge} = \sqrt[3]{\frac{\pi}{48\sqrt{2}}}d_{gr} = \beta_e d_{gr} \approx 0.359 d_{gr}, \tag{2}$$

where d_{gr} is the grain diameter, so, the typical value for L_{edge} is 3-4 μm.

The surface density of the grain face bubbles was measured in several independent tests (e.g. [2,11]) and turned out to vary in

* Corresponding author. Tel.: +7 (495) 955 2218; fax: +7 (495) 958 0040.
E-mail address: vms@ibrae.ac.ru (M.S. Veshchunov).

0022-3115/$ - see front matter © 2009 Elsevier B.V. All rights reserved.
doi:10.1016/j.jnucmat.2009.03.056

the range 10^{11}–10^{13} m^{-2}. The analysis of the available data demonstrates that ρ_f can be fairly well approximated in a wide temperature interval 800–1900 °C by the formula:

$$\rho_f = \min\{\rho_0 \exp(T_0/T), \rho_{\max}\}, \tag{3}$$

where $\rho_{\max} = 10^{13}$ m^{-2}, $\rho_0 = 3.67 \cdot 10^8$ m^{-2}, $T_0 = 13140$ K.

After foreseen implementation in the MFPR code of the intergranular coalescence model, recently developed by the authors [12], more realistic consideration of the bubble surface density will be accomplished in the code.

As for grain edge bubbles, simulation of their concentration is a complex problem requiring consideration of coalescence/collapse processes mentioned in Part 1. Therefore, in the lack of detailed systematic data the simplified model is utilized assuming that the mean distance L_{ee} between the grain edge bubbles is proportional to that between the grain face bubbles:

$$L_{ee} = 2\zeta_e R_s, \tag{4}$$

where $R_s = (\pi\rho_f)^{-1/2}$ is the radius of a sink-free region (see Part 1) and ζ_e is the model free parameter. Therefore, the surface density ρ_e of the edge bubbles can be calculated as:

$$\rho_e = \frac{3N_{epg}L_{edge}}{2\zeta_e R_s \pi d_{gr}^2} = \frac{18\beta_e(\pi\rho_f)^{1/2}}{\pi\zeta_e d_{gr}}, \tag{5}$$

where the coefficient $\beta_e \approx 0.359$ was introduced in Eq. (2).

As mentioned in Part 1, the grain face bubbles are formed by intersection of two spherical surfaces of radius R_f and hence have a circular projection [10] with the projected radius

$$\widetilde{R}_f = R_f \sin\theta, \tag{6}$$

and the correction factor for the volume, $V_f = \frac{4}{3}\pi R_f^3 f_f(\theta)$,

$$f_f(\theta) = 1 - \frac{3}{2}k + \frac{1}{2}k^3, \tag{7}$$

where

$$k = \cos\theta \approx \cos 50^\circ \approx 0.64, \tag{8}$$

θ being the semi-dihedral angle.

The edge bubbles are usually considered as cigar-shaped formed by intersection of three spherical surfaces of radius R_e. The length l_e of an edge bubble is connected with its radius of curvature by the relationship [10]

$$l_e = 2R_e\sqrt{1 - \frac{4k^2}{3}}, \tag{9}$$

and the volume correction factor is

$$f_e = \frac{3}{2\pi}\left[\pi - 2\arcsin\left(\frac{1}{2\sqrt{1-k^2}}\right) + \frac{k^2}{3}\sqrt{3-4k^2} - k(3-k^2)\arccos\left(\frac{k}{\sqrt{3(1-k^2)}}\right)\right]. \tag{10}$$

However, such complicated description of the bubble shape does not comply with the above formulated simplified description of the edge bubble concentration. Therefore, the form of the grain edge bubbles is further assumed to be spherical one with the radius R_e. The same approach was adopted for the corner bubbles as well. Moreover, for simplicity the edge and corner bubbles will be further considered as indistinguishable and the peripheral porosity will be represented only by one kind (edge) of the bubbles.

2.2. Coverage factors

The coverage factors, φ_f and φ_e, for the face and edge bubbles are defined as:

$$\varphi_{f,e} = S_{f,e}\rho_{f,e}, \tag{11}$$

where $S_{f,e}$ and $\rho_{f,e}$ are the area of the bubble projection on the grain surface and the bubble surface density, respectively.

The projection area of the grain face bubble is calculated as $S_f = \pi\widetilde{R}_f^2$. To estimate S_e one takes into account that each edge bubble is shared by three grains. Therefore, the bubble projection within one grain can be approximated by an ellipse with the semi-major and semi-minor axes R_e and $\sqrt{3}R_e/2$, respectively, so that the projection area is evaluated as:

$$S_e \approx \pi(\sqrt{3}/2)R_e^2 \approx 0.866\pi R_e^2. \tag{12}$$

So, the formulas for the coverage factors of the grain face and edge bubbles take the form:

$$\varphi_f = \pi\rho_f(R_f\sin\theta)^2,$$
$$\varphi_e = \frac{9\sqrt{3\pi}\beta_e\rho_f^{1/2}R_e^2}{\zeta_e d_{gr}} \approx 9.92\frac{\rho_f^{1/2}R_e^2}{\zeta_e d_{gr}}. \tag{13}$$

The grain face bubbles interlinkage leading to formation of channels connected with open porosity at edges is supposed to be attained when the projected area coverage of the grain face bubbles φ_f exceeds the critical value $\varphi_f^{(cr)} = 0.5$, roughly corresponding to the 2-d percolation threshold (see Part 1).

The grain edge porosity interlinkage leading to formation of escape tunnels takes place when these bubbles are just touching each other (the 1-d percolation threshold); with Eq. (4) taken into account, the condition of the onset of the escape tunnels takes the form:

$$R_e = \zeta_e R_s = \zeta_e(\pi\rho_f)^{-1/2}. \tag{14}$$

As explained in Part 1 (Section 4.5), after attainment of the percolation threshold the tunnel radius continuously increases owing to gas venting and coalescence of the edge bubbles. On the other hand, coalescence of the face bubbles leads to a continuous decrease of ρ_f. In the simplest approximation accepted in the current paper the coalescence rates either of the face or of the edge bubbles are neglected, and, therefore, Eq. (14) is valid also in this "venting" stage. For this reason, the steady-state value of the face bubbles coverage factor, attained after the edge tunnels formation and obeying the relationship $\varphi_f^{(ss)} \propto R_e/R_s$ (derived in Part 1), turns out to be a constant value. However, in a more realistic approach both coalescence processes should be included in consideration (as foreseen in the future development of the MFPR code, see also [12]). This will result in a smooth variation of the steady-state face bubbles coverage factor $\varphi_f^{(ss)}$ with time and temperature, which can generally attain the percolation threshold value of ≈0.5 (e.g. under high temperature conditions owing to significant growth of R_e).

2.3. Resolution from non-spherical bubbles

According to Nelson's model [13], the resolution rate does not depend on the size of small (Van der Waals) bubbles. For larger spherical bubbles of radius R_b only a fraction of gas atoms within a critical distance from the bubble surface Δ may escape. Therefore the resolution kinetic parameter is calculated as:

$$\omega_{rsi}^{Nelson}(R_b) = G b_0 \cdot \begin{cases} 1 & \text{for} \quad y = \Delta/R_b \geqslant 1, \\ 3y(1 - y + y^2/3) & \text{for} \quad y = \Delta/R_b < 1, \end{cases} \tag{15}$$

where G is the fission rate, $b_0 \approx 2 \cdot 10^{-23}$ cm^3 is the resolution constant. Supposing that the minimal energy that a struck gas atom must receive to be trapped by surrounding lattice is 300 eV, the value of Δ can be estimated as 1.0–1.5 nm [13]. In the VICTORIA [6] and FASTGRASS [14] codes the modified model was implemented that introduced, instead of Δ, the average distance λ that an ejected atom travels in the bubble. So for the spherical bubbles one gets:

$$\omega_{rsi}(R_b) = G b_0 \cdot \begin{cases} 1 & \text{for} \quad z = \lambda/2R_b \geqslant 1, \\ \frac{1}{2} z(3 - z^2) & \text{for} \quad z = \lambda/2R_b < 1. \end{cases} \tag{16}$$

As seen the both formulas coincide for small bubbles; whereas for large bubbles they coincide asymptotically, provided $\lambda = 4\Delta$, in a reasonable agreement with the VICTORIA's value $\lambda = 5$ nm.

However these parameters cannot be considered as universal ones applicable to all bubbles. Indeed, the energy loss of the struck atom is determined by the number of collisions it had before it escapes the bubble. Therefore, the track length increases with the increase of inter-atomic distance within the bubble, which, in turn, increases with the bubble size. The universal scaling of the track length is determined by the formula:

$$\lambda = 1/n\sigma, \tag{17}$$

where n is the (number) density of the media and σ is the effective cross section of the collisions. The above mentioned parameter λ (hereafter referred to as λ_{VdW}) was introduced in [13] for the small bubbles for which $n \approx 1/B_{Xe}$, where B_{Xe} is the Van der Waals constant for xenon. Therefore, one evaluates σ value as B_{Xe}/λ_{VdW} and derives an approximate relation between the basic scale parameters of the model:

$$\lambda = \frac{V_b}{N_b \sigma} = \frac{\lambda_{VdW} V_b}{B_{Xe} N_b}, \tag{18}$$

where λ_{VdW} can be considered as a model free parameter (Nelson's estimate is ~5 nm), V_b and N_b are the bubble volume and number of atoms in the bubble.

For large grain face bubbles obeying the ideal gas law with the equilibrium pressure $p = 2\gamma/R_b$, where γ is the surface tension, Eq. (18) reduces to:

$$\lambda = \lambda_{VdW} \frac{kTR_b}{2\gamma B_{Xe}}. \tag{19}$$

For instance, in the case of $R_b = 10^{-7}$ m and $T = 1200$ K one gets $\lambda \approx 40$ nm, that is eight times greater than for the Van der Waals bubbles. Also, it is seen from this equation that for the large bubbles the ratio λ/R_b depends only on temperature.

The above Eqs. 15 and 16 were derived for spherical bubbles, for which the shapes correspond to the minimal surface area at fixed bubble volume and therefore to the minimal resolution intensity. For lenticular bubbles the relative bubble volume, from which atoms can escape, increases owing to the bubble specific geometry, therefore resolution kinetic coefficient should be modified. For large bubbles ($R_b \gg \lambda$) Eq. (16) can be rewritten in the form:

$$\omega_{rsi}(R_b) = G b_0 \frac{3\lambda}{4R_b} = G b_0 \frac{S_b}{V_b} \frac{\lambda}{4},$$

so, that taking into account the equations for the volume V_b of a lenticular bubble, Eq. (7), and for the bubble surface, $S_b = 4\pi R_b^2 (1 - \cos\theta)$, one derives that

$$\omega_{rsi}(R_b) = \frac{3\lambda G b_0}{4R_b(1 - \frac{1}{2}\cos\theta - \frac{1}{2}\cos^2\theta)} = \frac{\omega_{rsi}^{spherical}(R_b)}{1 - \frac{1}{2}\cos\theta - \frac{1}{2}\cos^2\theta}. \tag{20}$$

It is seen from this equation that the angle factor is always greater than one. In particular, for the face bubbles with $\theta \approx 50°$ consideration of the bubble shape correction results in an increase of the resolution intensity by a factor of 2.1 comparing with the spherical bubble with the same curvature radius R_b. Furthermore, in accordance with Part 1 (Section 4.2), the additional factor, $(1 - \gamma_e)$, will be introduced in Eq. (20) for the edge bubbles simulating the suppression of resolution mechanism, $\gamma_e < 1$ being considered as the model parameter.

3. Model validation

In order to simulate the experimental observations, the model for intergranular transport was implemented in the MFPR code [7,8]. In the modified code the intragranular FP transport was described in the framework of basic MFPR approach but with the modified boundary conditions (as described in Part 1). The output diffusion flux is then redistributed between intergranular sinks in accordance with the new intergranular transport model. The new model parameters γ_e, $\rho_{\max}$ and ζ_e were fitted against the experimental data [1,11] on grain face bubble sizes and concentrations, as described below in Sections 3.1 and 3.2. After this, the model with the fixed set of the parameters was verified against the CONTACT tests [15], as described in Section 3.3.

3.1. Tests of Kashibe and Une

There are several experimental works where microscopic behaviour of intergranular bubbles was observed directly [1,11]. As described in Part 1, in [1] the specimens were taken from UO_2 pellets irradiated in commercial BWR (burnup 6–28 GWd/t) at a point between the fuel periphery and middle. Grain face bubble concentration and fractional coverage were examined by scanning electron microscope fractography. The grain sizes of the fuel and irradiation rate were approximately equal to 9 μm and $1.8 \cdot 10^{19}$ m^{-3}s^{-1}, correspondingly. In the lack of temperature measurements in these tests, one can evaluate the irradiation temperature at the location of the specimens as ~1500 K from the maximum linear heat generation rates between 30 and 37 kW/m.

As above explained, the new intergranular model has three unknown dimensionless parameters: the suppression factor γ_e for resolution flux from edge bubbles, Eq. (4) from Part 1, the track length λ_{VdW}, Eq. (18), and the ratio ζ_e of the average distance between edge bubbles to that between face bubbles, Eq. (4). Variation of these parameters has revealed that λ_{VdW} had a weak effect on the model predictions, so it was fixed at the value of 5 nm, following Nelson's estimate of 4-6 nm (see Section 2.3). The other parameters were chosen to provide the correct description of the Une and Kashibe data [1,2] at burnup 28 GWd/t. The found values are $\zeta_e = 0.2$, $\gamma_e = 0.67$.

In Table 1 the calculated grain face bubble characteristics: the coverage factor φ_f, the *Xe* fractional release f_{Xe}, the surface density ρ_f and the mean projection diameter $d_f = 2\widetilde{R}_f$ of the grain face bubbles are compared with the experimental data.

As seen, in general the model adequately describes the experimental data with some underestimation of the grain face coverage and small overestimation of the face bubble density. However, it should be noted that the data [1,2] are quite widely scattered from

Table 1
Characteristics of the grain face bubbles in simulation of the Kashibe–Une tests [1,2].

	φ_f (%)	f_{Xe} (%)	ρ_f (m^{-2})	d_f (nm)
Model	8.4	35	$2.1 \cdot 10^{12}$	229
Experiment	10.1	30-50	$1.6 \cdot 10^{12}$	229

grain to grain and the measured values may be considered only as estimations.

3.2. Tests of Pati et al.

In experiment [11] of Pati et al. the UO_2 fuel irradiated to a burnup of $2 \times 10^{26}\,m^{-3}$ with fission rate $\approx 2.6 \times 10^{19}\,s^{-1}\,m^{-3}$ was examined by transmission and scanning electron microscopy and replication metallography. In these tests gas release was not measured, however, the fission gas distribution on the grain boundaries was characterized as a function of irradiation temperature 750–1350 °C. In Fig. 1 the calculated temperature dependences of the volume density C_f (upper panel) and projection radius $\widetilde{R}_f$ (lower panel) of intergranular bubbles are compared with the experimental data.

As seen, the MFPR correlation reasonably describes the temperature dependence of the concentration of the grain face bubbles at high temperatures while overestimates the experiment for temperatures below ~1250 K. In fact, the concentration is calculated using simple correlation, Eq. (3), with the cut-off surface density ρ_{max}, which was set equal to $10^{13}\,m^{-2}$ in the original model to fit Pati's data. However, this restriction is inconsistent with other data. For instance, Kashibe and Une [1] observed the concentrations up to $6 \cdot 10^{13}\,m^{-2}$ (at temperature 1400–1600 K) that corresponds to the volume density of $C_f = 2 \cdot 10^{19}\,m^{-3}$, more that one order of magnitude higher than presented in Fig. 1. For this reason, in the present version the parameter ρ_{max} was increased up to $6 \cdot 10^{13}\,m^{-2}$.

As for the bubble sizes, the MFPR results underestimate the experimental data by a factor of ~3. However, there is also a disagreement with the measured projection bubble radii in the tests [1] under similar conditions. Indeed, the value of Kashibe and Une was $229/2 \approx 115$ nm at $T = 1523$ K (cf. Table 1) that is three times less than Pati's value, whereas the inverse ratio takes place for the burnups (3.3% for the test of Kashibe and Une and 0.8% for Pati's test.). So, in the MFPR simulations more recent experimental data [1,2] are considered as more precise and reliable.

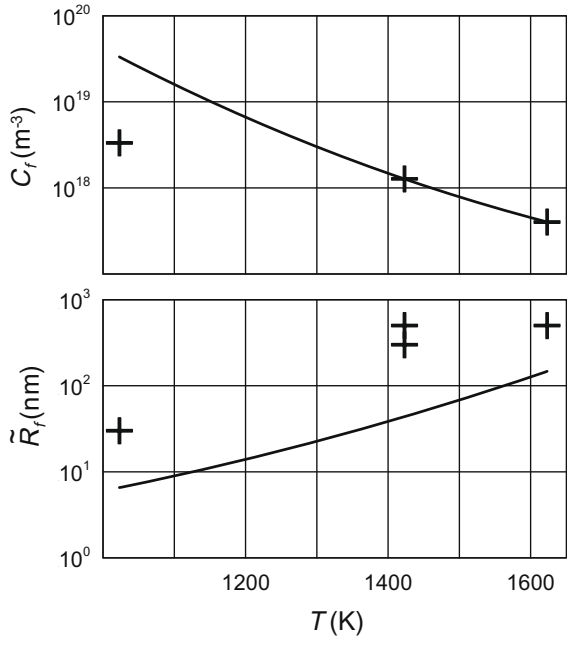

Fig. 1. Dependence of the volume density C_f and projection radius $\widetilde{R}_f$ of intergranular bubbles on temperature under conditions of the test [11]; curves and markers correspond to MFPR results and experimental data, respectively.

3.3. CONTACT tests

The CONTACT series of experiments was a program of in-pile tests conducted in the SILOE reactor in Grenoble, France, funded jointly between CEA and Framatome [15,16]. Short rods with Zry-4 clad UO_2 pellets of typical PWR 17×17 design were irradiated under conditions designed to simulate those of commercial PWRs. Each rod was equipped with a fuel centerline thermocouple, diameter gauge, gas lines providing a flow of gas through the rod and internal pressure gauges to measure pressure drop along the fuel stack. The gas flow entrained released fission gases which were measured by a gamma detector installed in the out-of-reactor gas handling system. The experiment is unique in that the rods operated under near constant powers for the majority of their lives.

CONTACT 1 operated at a constant 40 kW/m up to a burn-up of ~22 MWd/kgU. The data include temperatures as a function of burn-up, clad diameter changes as a function of power and burn-up, stable and radioactive fission gas release as a function of center temperature and burn-up.

In calculations, the grain size, fission rate and internal pressure were set equal to 10 μm, 10^{19} fissions/m^3 s and 1 MPa, respectively, in accordance with the experimental data. The centerline temperatures were measured to be rather stable (within ±4%) near 1747 K during all irradiation period. From these data, the temperature profile in the pellet was calculated using the heat conductance model of the SVECHA code [17] with the urania thermal conductivity from [18], Fig. 2.

On this base, the burnup dependence of gas fractional release is calculated with the fixed set of the new model parameters and compared with the experiment in Fig. 3, demonstrating reasonable predictions of the code for gas release under steady irradiation conditions.

Note that the calculated curve in Fig. 3 corresponds to the fractional release averaged over the pellet. As for local release, it is ≈0.72 in the central part of the pellet and decreases toward the pellet periphery. Roughly, only a central half of the pellet volume contributes to the release while there is no release from the outer regions.

It should be emphasized that the local coverage factors φ_f is almost constant (varying from 0.082 to 0.088) within the release region, in agreement with the theoretical considerations in Section 4.5 of Part 1. This indicates that the gas release is associated with the diffusion mechanism over the grain surface rather than with the percolation network, in a qualitative agreement with observations in the same temperature range (for the MOX fuel), presented in Section 5 of Part 1.

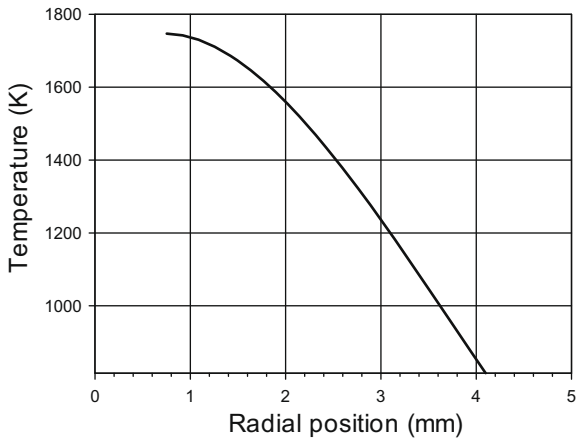

Fig. 2. Radial distribution of temperature in UO_2 pellet in the CONTACT 1 test calculated with the SVECHA code [17].

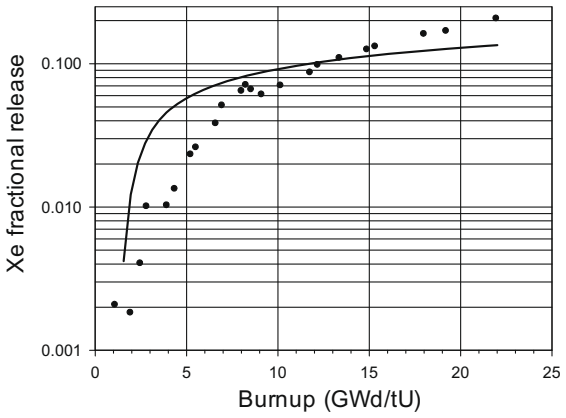

Fig. 3. MFPR simulations (curve) of cumulative fractional gas release in the CONTACT 1 test, markers representing the experimental data [15,16].

As explained in Section 2.2, in a more realistic approach when the edge and face bubbles coalescence processes are taken in consideration, the local coverage factors φ_f will smoothly increase with time and in the hot zone of the pellet can even attain the saturation coverage manifested by formation of the face bubbles network interconnected with the escape tunnels. This consideration is foreseen in the close future.

4. Conclusions

The model for intergranular diffusion transport in irradiated UO_2 fuel described in Part 1 was numerically realised. The important model parameters including the shape, size and concentration of the intergranular bubbles were specified, and improvement of the model for the irradiation induced re-solution of gas atoms from these bubbles was carried out.

Implementation of the advanced model in the MFPR code and numerical treatment of various available data on gas release from irradiated fuel and grain face microstructure show a satisfactory agreement of the code predictions with the experimental results. In particular, the modified code allows description of the Kashibe and Une test in satisfactory agreement with the measurements of the fractional gas release along with the bubbles sizes and grain face coverage. As a result, the main model prediction concerning the onset of gas release from the fuel at very low grain face bubble coverage, below the saturation value manifested by formation of bubble network on grain faces interconnected with open porosity, was confirmed by calculations. Using this model, a satisfactory agreement was demonstrated of the model predictions with the measured fractional release in the SILOE reactor tests under well-controlled steady irradiation conditions.

Acknowledgements

This work was supported by IRSN, Cadarache (France) under the Contract on the mechanistic code MFPR development; the personal support and collaboration of Dr R. Dubourg and Dr P. Giordano (IRSN) are highly appreciated. The authors also thank Dr V. Ozrin (IBRAE) for collaboration in implementation of the new model in the MFPR code and Dr V.E. Shestak (IBRAE) for calculations with the SVECHA code. Dr G. Ducros (CEA, Cadarache) is greatly acknowledged for presentation of relevant publications on the CONTACT tests.

This work was also supported by the Russian Foundation for Basic Research, which is greatly acknowledged by the authors.

References

[1] K. Une, S. Kashibe, J. Nucl. Sci. Technol. 27 (1990) 1002.
[2] S. Kashibe, K. Une, J. Nucl. Sci. Technol. 28 (1991) 1090.
[3] R.J. White, M.O. Tucker, J. Nucl. Mater. 118 (1983) 1.
[4] K. Forsberg, A.R. Massih, J. Nucl. Mater. 135 (1985) 140.
[5] C.C. Dollins, F.A. Nichols, J. Nucl. Mater. 91 (1976) 143.
[6] T.J. Heames, D.A. Williams, N.E. Bixler, A.J. Grimley, C.J. Wheatley, N.A. Johns, P. Domogala, L.W. Dickson, C.A. Alexander, I. Osborn-Lee, S. Zawadzki, J. Rest, A. Mason, R.Y. Lee, VICTORIA: A Mechanistic Model of Radionuclide Behaviour in the Reactor Coolant System Under Severe Accident Conditions, NUREG/CR-5545, 1992.
[7] M.S. Veshchunov, V.D. Ozrin, V.E. Shestak, V.I. Tarasov, R. Dubourg, G. Nicaise, Nucl. Eng. Des. 236 (2006) 179.
[8] M.S. Veshchunov, R. Dubourg, V.D. Ozrin, V.E. Shestak, V.I. Tarasov, J. Nucl. Mater. 362 (2007) 327.
[9] M.O. Tucker, J. Nucl. Mater. 89 (1979) 199.
[10] P.J. Clemm, J.C. Fisher, Acta Metall. 3 (1955) 70.
[11] S.R. Pati, M.J. Dapt, D.R. O'Boyle, J. Nucl. Mater. 50 (1974) 227.
[12] M.S. Veshchunov, J. Nucl. Mater. 374 (2008) 44.
[13] R.S. Nelson, J. Nucl. Mater. 31 (1969) 153.
[14] J. Rest, S.A. Zawadzki, FASTGRASS, A Mechanistic Model for the Prediction of Xe, I, Cs, Te, Ba and Sr Release from Nuclear Fuel under Normal and Severe-Accident Conditions, NUREG/CR-5840 TI92 040783, 1994.
[15] M. Bruet, J. Dodelier, P. Melin, M. L. Pointud, in: IAEA Specialists' Meeting on Water Reactor Fuel Element Performance Computer Modelling, Blackpool, 17-21 March 1980.
[16] M. Charles, J.J. Abassin, D. Baron, M. Bruet, P. Melin, in: Water Reactor Fuel Element Performance Computer Modelling, Elsevier Science Ltd., 1983.
[17] P. Hofmann, V. Noack, M.S. Veshchunov, A.V. Berdyshev, A.V. Boldyrev, L.V. Matweev, A.V. Palagin, V.E. Shestak, Physico-Chemical Behavior of Zircaloy Fuel Rod Cladding Tubes During LWR Severe Accident Reflood, Report FZKA 5846, Karlsruhe, Germany, 1997.
[18] K. Ohira, N. Itagaki, in: Proceedings of the ANS International Topical Meeting on LWR Fuel Performance, 2–6 March 1997, Portland, Oregon, 1997, p. 541.